

# Atomic Force Microscopy Reveals Differences In Mechanical Properties Linked To Cortical Structure In Mouse And Human Oocytes

Rose Bulteau, Lucie Barbier, Guillaume Lamour, Yassir Lemseffer, Marie-Hélène Verlhac, Nicolas Tessandier, Elsa Labrune, Martin Lenz, Marie-Emilie Terret,\* and Clément Campillo\*

Cell mechanical properties regulate biological processes such as oocyte development. Cortical tension is regulated via actomyosin cortex remodeling to ensure optimal oocyte quality. However, the evolution of other mechanical parameters and their relationship with cortex structure remain poorly understood in mammalian oocytes. In this work, a methodology combining multiple mechanical parameters measured through Atomic Force Microscopy is proposed to investigate the relationship between oocyte mechanical properties and cortex organization. By studying mouse oocytes at various stages of development, along with engineered ones with specific cortex organization, it is demonstrated that a thin actin cortex corresponds to stiff oocytes while a thick one is associated with softer oocytes. It is further revealed that maternal age, a critical factor for fertility, affects mouse oocytes mechanics, correlating with alterations in their cortex structure. Finally, it is shown that the evolution of mechanical properties differs between human and mouse oocyte development, highlighting species-specific differences in cortex organization.

## 1. Introduction

Living cells are complex materials whose mechanical properties evolve during biological processes such as cell division<sup>[1]</sup> and during the evolution of pathologies such as cancer.<sup>[2,3]</sup> Mechanical properties of the cell surface are modulated by the cell cortex, an actin-rich structure lying beneath the plasma membrane, in which actin filaments are nucleated at the membrane and interact with myosin motors.<sup>[4]</sup> Cortical tension is a mechanical property that corresponds to the energy required to increase the cell surface<sup>[5]</sup> and is determined by the dynamics of actin polymerization and myosin activity.<sup>[6]</sup> It has been shown that cortical tension is tightly regulated during the final phase of mouse oocyte

R. Bulteau, G. Lamour, C. Campillo

LAMBE

Univ Evry

CNRS

Université Paris-Saclay

Évry-Courcouronnes 91025, France

E-mail: [clement.campillo@univ-evry.fr](mailto:clement.campillo@univ-evry.fr)

R. Bulteau, L. Barbier, M.-H. Verlhac, N. Tessandier, M.-E. Terret

Center for Interdisciplinary Research in Biology (CIRB)

Collège de France

Université PSL

CNRS

INSERM

Paris 75005, France

E-mail: [marie-emilie.terret@college-de-france.fr](mailto:marie-emilie.terret@college-de-france.fr)

M. Lenz

LPTMS

CNRS

Université Paris-Sud

Université Paris-Saclay

Orsay 91405, France

Y. Lemseffer, E. Labrune

Hospices Civils de Lyon

service de médecine de la reproduction et préservation de fertilité;

Inserm U1208

SBRI

Université Claude Bernard Lyon 1

faculté de médecine

Laennec, France

C. Campillo

Institut Universitaire de France (IUF)

Paris 75005, France

 The ORCID identification number(s) for the author(s) of this article can be found under <https://doi.org/10.1002/smll.202500221>

© 2025 The Author(s). Small published by Wiley-VCH GmbH. This is an open access article under the terms of the [Creative Commons](#)

[Attribution-NonCommercial-NoDerivs](#) License, which permits use and distribution in any medium, provided the original work is properly cited, the use is non-commercial and no modifications or adaptations are made.

DOI: 10.1002/smll.202500221

development, called meiotic maturation.<sup>[7,8]</sup> At birth in mammals, oocytes are arrested in prophase of the first meiotic division (prophase I, PI). After puberty and cyclically, some oocytes undergo meiotic maturation: they exit from prophase I, complete the first meiotic division (meiosis I, MI), and arrest in metaphase of the second meiotic division (meiosis II, MII) until fertilization. After meiosis I entry, the oocyte cortex gradually thickens through actin nucleation, chasing cortical myosin-II and leading to a decrease in cortical tension.<sup>[7]</sup> Aberrant low or high cortical tension, a frequent defect in mammalian oocytes<sup>[9]</sup> can hinder division geometry and induce aneuploidy.<sup>[10,7,11]</sup> These studies show that the actomyosin cortex is a key factor for proper oocyte formation and that cortical tension measurements may indicate alterations in the actomyosin cortex structure. However, how other mechanical parameters, such as elasticity and viscosity, evolve with changes in the actomyosin cortex is still unknown.

Atomic Force Microscopy (AFM) is a robust method for probing multiple mechanical properties of living cells surface.<sup>[3,12–20]</sup> In AFM experiments, the cell is probed by a nanometer-sized tip located at the end of a flexible cantilever. To measure mechanical parameters, the tip presses on the cell, inducing a local deformation. The force applied and the resulting cell deformation are recorded through the cantilever deflection, producing force-indentation curves. Fitting these force-indentation curves with appropriate physical models gives access to the cell's mechanical properties. In most studies, living cells are treated as bulk elastic materials, and their effective elastic modulus is extracted from these curves.<sup>[21,22]</sup> Only a few studies use local AFM indentation to measure cell cortical tension.<sup>[23,24]</sup> The respective contributions of elastic modulus and tension on the cell cortex response in AFM experiments are unclear. Moreover, the cell internal medium also dissipates energy, as shown in AFM experiments by the difference between approach and retract curves.<sup>[25]</sup> Few works have assessed oocyte mechanical properties using AFM. In most cases, they have probed the *Zona Pellucida*, the porous network of glycoproteins constituting the extracellular matrix surrounding mammalian oocytes, using purely elastic models.<sup>[26–28]</sup> Some have probed the mechanical contributions associated with the *Zona Pellucida* and the whole oocyte,<sup>[29,30]</sup> using time-relaxation measurements with flat macro-cantilevers.<sup>[28]</sup> However, AFM measurements directly probing the oocyte cortex have not been performed and could extend the current description of oocyte mechanics. Moreover, existing mechanical studies of oocytes are limited to a single mechanical parameter, such as elastic modulus or cortical tension.

Here, we propose a methodology that combines several mechanical parameters obtained through Atomic Force Microscopy experiments to study the links between oocyte's mechanical properties and actin cortical organization. We developed an elasto-capillary model and analysis pipeline that allows extracting oocyte elastic modulus, cortical tension, and energy dissipation. We confirmed that our model accurately describes oocyte force-indentation response and yields values of cortical tension consistent with the ones obtained by micropipette aspiration.<sup>[7,8,31]</sup> We investigated different stages of mouse oocyte maturation and engineered mouse oocytes in which the actomyosin cortex is manipulated to obtain oocyte models with increased or decreased cortical tension. Using principal component analysis combining the parameters obtained by AFM, we found that groups of oocytes

cluster depending on their actin cortical organization. Importantly, we also described this link between actin cortical organization and mechanical properties in the subfertile case of mouse advanced maternal age and in human oocytes. However, the evolution of the mechanical properties during meiotic maturation differed between human and mouse oocytes, suggesting different molecular regulation.

## 2. Results

### 2.1. Describing Oocyte Mechanics with an Elasto-Capillary Model

We used the AFM measurement technique adapted to mammalian oocytes, which we recently developed<sup>[32]</sup> (Figures 1A, and S1, Supporting Information). To probe the oocyte cortex without the mechanical contributions associated with the *Zona Pellucida*, we performed the measurements after removing this layer (Figure S2A, Supporting Information). We indented the top of the oocyte and monitored the compression force  $\mathcal{F}$  as a function of the oocyte indentation  $\delta_{\text{tot}}$ . We first gradually compressed the oocyte by lowering the indenter over the course of seconds up to a maximal applied force set at 0.5 nN, then raised the indenter again. We thus collected two force-indentation curves corresponding to the approach and the retract phases (Figure 1B). From these force curves, we can extract several mechanical parameters.

The approach and retract curves do not overlap, revealing a viscous energy dissipation during the indentation. We calculate this dissipated energy by integrating the area between the approach and the retract curves (Figure 1B). This quantity is normalized by the area under the approach curve.<sup>[25]</sup> It thus provides a dimensionless quantity close to 1 in cases of high viscous dissipation and 0 for low dissipation. These values range from 0.4 to 0.6, showing that both dissipative and non-dissipative contributions must be considered in the oocyte's mechanical description.

To infer information about the non-dissipative part of the oocyte's mechanical response, we consider the approach indentation curve (performed on a mouse oocyte with an average radius of 36.5  $\mu\text{m}$  and a cortex with an average thickness of 2  $\mu\text{m}$ ) and note that it combines characteristics of the response of two distinct non-dissipative elements, one at small indentation and the other at large ones (Figure 1C). For small indentations, it displays a parabolic dependence of the force on the indentation. This is consistent with the response of a purely elastic homogeneous and isotropic half-space indented by a pyramidal probe without adhesion. In such a setting, the standard Sneddon model<sup>[33]</sup> predicts that the indentation force depends on the indentation  $\delta_e$  of the elastic half-space through:

$$\mathcal{F} = E^* (\delta_e)^2 \quad (1)$$

where the characteristic modulus  $E^* = 0.887 \tan(\alpha) \frac{E}{1-\nu^2}$  is a function of the elastic modulus  $E$ ; the Poisson ratio  $\nu = 0.5$  (assuming an incompressible material) and the side angle  $\alpha = 17.5^\circ$  of the indenter cone. We chose this simple model as an approximation to describe the elastic response of the oocyte surface because our experiments are in the limit of low indentation rate, on the order of a few percent. Indeed, the oocyte diameter without the *Zona*

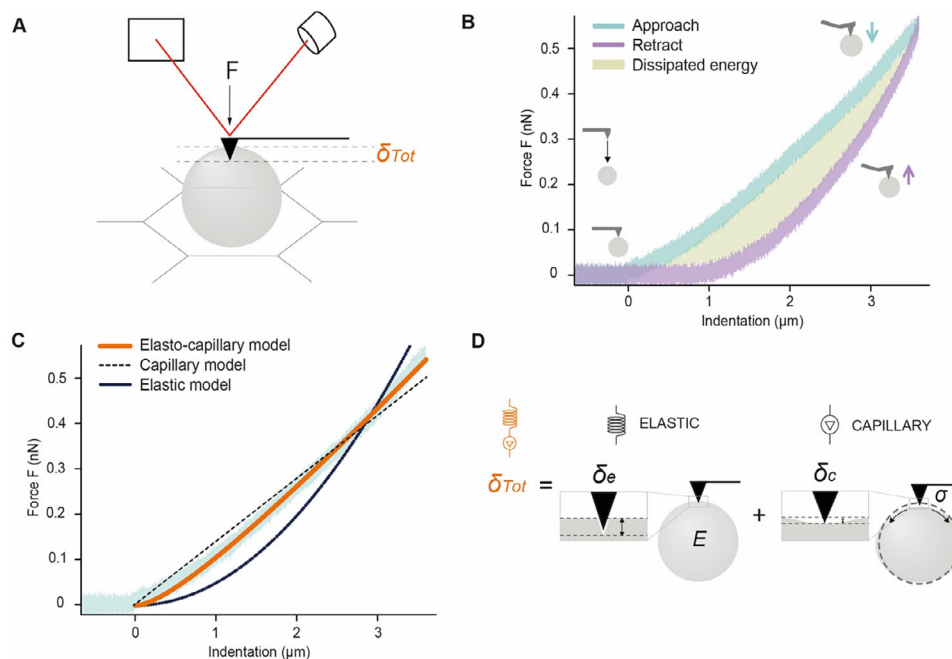


**Figure 1.** AFM measurement of mammalian oocyte mechanics: strategy, modeling, and analysis. A) Scheme of the AFM measurement technique (oocyte in grey placed on an electronic microscopy grid, laser in red). B) Example of a representative approach (blue) and retract (purple) force-indentation curve obtained for one oocyte. The green area between the approach and retract curves corresponds to the dissipated viscous energy. C) Graph showing the force-indentation curve fits with an elastic model (continuous black line), a capillary model (black dashed line), and the elasto-capillary model (orange line), which is used to extract oocyte cortical tension and elastic modulus. D) The total indentation in the oocyte ( $\delta_{Tot}$ ) is the sum of the elastic ( $\delta_e$ ) and capillary ( $\delta_c$ ) indentations. The oocyte (in grey) is described mechanically as a spring and a contractile element in series.

*Pellucida* is  $\approx 73$  micrometers in mice (115 micrometers in humans), therefore, the ratio between indentation depth and cell diameter is a maximum of 8% for mouse oocytes and 5% for human oocytes. For larger indentations, the force appears to depend affinely on the indentation. This is consistent with the capillary response of a disk of membrane-like thin elastic slab under tension indented over a depth  $\delta_c$ ,<sup>[34]</sup> namely:

$$F = \sigma^* \delta_c \quad (2)$$

This expression involves a characteristic tension  $\sigma^* = \frac{2\pi\sigma}{\gamma + \ln[2R\sqrt{\frac{3(1-\nu^2)\sigma}{Eh^3}}]}$ , which features the cortical tension  $\sigma$ , the Euler gamma constant  $\gamma \approx 0.577$ , the radius  $R$  of the membrane disk and the thickness  $h$  of the membrane. While  $\sigma^*$  depends on many parameters, for large enough membranes, the logarithmic dependence of its denominator is very weak and thus  $\sigma^*$ , for typical values of experimental parameters ( $R = 36.5\mu\text{m}$ ,  $h = 2\mu\text{m}$ ,  $E = 1\text{kPa}$ ,  $\sigma = 1\text{nN}\cdot\mu\text{m}^{-1}$ ), is equal to the cortical tension  $\sigma$ . The linear behavior of the curves in this case is in agreement with other studies.<sup>[23,35]</sup>

We rationalize this complex dependence of the force on the indentation through a geometric argument. We assimilate the oocyte cortex to a tense elastic shell whose thickness  $h$  is much smaller than its radius  $R$ . In such a setting, the cortex deformation induced by the indenter involves two widely different length scales (Figure 1D). At a very local scale, the tip of the indenter penetrates into the cortex by a distance  $\delta_e$ , i.e., the distance between the tip and the cortex mid-plane is  $h/2 - \delta_e$ . On larger length

scales, the downward force exerted by the indenter additionally pushes this midplane down by a distance  $\delta_c$ , implying that over length scales much larger than  $h$ , the cortex acts as a tense membrane subjected to a downward point force. We reason that the total indentation  $\delta_{tot}$  of the oocyte is the sum of these local and large-scale displacements, implying

$$\delta_{tot} = \delta_e + \delta_c \quad (3)$$

Inserting Equations (1) and (2) yields the following expression for the total indentation:

$$\delta_{tot} = \sqrt{\frac{F}{E^*}} + \frac{F}{\sigma^*} \quad (4)$$

which leads to:

$$F = \left( \sqrt{\delta_{tot}\sigma^* + \frac{\sigma^{*2}}{4E^*}} - \sqrt{\frac{\sigma^{*2}}{4E^*}} \right)^2 \quad (5)$$

with which we fit our approach curve (Figure 1C,D). Equation (3) is parabolic at low indentation and thus dominated by the elastic response. As expected, this expression crosses over from a parabolic elastic-dominated response for  $\delta \ll \frac{\sigma}{E^*}$  to a linear capillary regime for  $\delta \gg \frac{\sigma}{E^*}$ . This elasto-capillary model accurately fits our force curves in the approach phase (Figure 1D), and the Residual Standard Errors (RSE) are lower as compared to elastic or capillary models (Figure S2B, Supporting Information).

Therefore, our measurements simultaneously provide values of oocyte elastic modulus  $E$  and cortical tension  $\sigma$ .

To quantify the elastic vs. capillary character of the oocytes in our conditions of indentation, we introduce a dimensionless parameter, which we name the capillary indentation ratio  $r_c$ :

$$r_c = \frac{\delta_c}{\delta_e + \delta_c} = \frac{\frac{F}{\sigma^*}}{\sqrt{F/E^*} + F/\sigma^*} \quad (6)$$

A ratio  $r_c = 0$  indicates that the oocyte has a purely elastic behavior. In contrast,  $r_c = 1$  corresponds to a purely capillary response. For 70% of our data,  $0.05 < r_c < 0.95$  at the maximum indentation force, implying a mixed behavior. In few cases, one of the two behaviors dominates the oocytes' mechanical response, implying that their response curves contain very little information about the other. In practice, in such cases, our fitting procedure returns unreliable values for the elastic parameter associated with the subdominant behavior (Figure S2C, Supporting Information). We thus disregarded these curves in the following.

Our AFM experiments and fitting procedure thus provide four mechanical parameters characterizing oocytes: normalized dissipated energy ( $DE$ ), cortical tension ( $\sigma$ ), elastic modulus ( $E$ ), and maximum capillary indentation ratio ( $r_c$ ).

## 2.2. Oocyte Mechanics Predict Cortex Organization

To validate our model and investigate the link between oocyte mechanics and cortex organization, we first probed mouse oocytes with known cortical tension and organization. We compared oocytes arrested in prophase I (PI), oocytes in meiosis I (in early or late MI), oocytes arrested in meiosis II (MII), and engineered oocytes with a modified cortex organization<sup>[7]</sup> (Figure 2A). These oocytes express cortical probes either forcing cortical actin nucleation and chasing cortical myosin-II (cVCA, lower cortical tension<sup>[11]</sup>) or forcing myosin-II recruitment at the cortex (cRhoA,<sup>[36]</sup> higher cortical tension - Figure S2D, Supporting Information). As a control, we used oocytes expressing only the cortical anchor (Ctrl). We characterized the mechanics of all these types of oocytes using AFM.

We first measured a decrease in cortical tension after meiosis I entry (Figure 2B,  $1.6 \text{ nN}\cdot\mu\text{m}^{-1}$  for PI vs.  $0.2 \text{ nN}\cdot\mu\text{m}^{-1}$  for late MI) and for cVCA oocytes (Figure 2B,  $0.25 \text{ nN}\cdot\mu\text{m}^{-1}$  for cVCA vs.  $1.1 \text{ nN}\cdot\mu\text{m}^{-1}$  for Ctrl). By contrast, we measured an increase in cortical tension for cRhoA compared to Ctrl oocytes (Figure 2B,  $1.8 \text{ nN}\cdot\mu\text{m}^{-1}$  for cRhoA vs.  $1.1 \text{ nN}\cdot\mu\text{m}^{-1}$  for Ctrl). These results are consistent with previous measurements of cortical tension obtained with micropipette aspiration,<sup>[7,8,10,11]</sup> validating the elastocapillary model.

Then, we assessed the three additional mechanical parameters described above. After meiosis I entry, the elastic modulus decreases progressively ( $4.6 \text{ kPa}$  for PI vs.  $0.5 \text{ kPa}$  for late MI) while the capillary indentation ratio increases. Normalized dissipated energy also decreases after meiosis I entry but returns in Meiosis II to values similar to those of oocytes in prophase I (Figure 2B). For engineered oocytes, the elastic modulus is similar for cRhoA ( $8.2 \text{ kPa}$ ) and lower for cVCA ( $0.4 \text{ kPa}$ ) than for Ctrl oocytes ( $5.2 \text{ kPa}$ ). The normalized dissipated energy is higher for cVCA oocytes and similar between cRhoA and Ctrl oocytes.

The capillary indentation ratio for cVCA oocytes is closer to a capillary-dominated response than for cRhoA ones (Figure 2B). Overall, while the elastic modulus seems to follow similar trends to cortical tension, the normalized dissipated energy and the capillary indentation ratio evolve independently in the different types of oocytes probed.

To facilitate the visualization of our multiparametric data set and possibly identify groups of oocytes with similar mechanical properties, we combined the four mechanical parameters in a principal component analysis (PCA) (Figure 2C). For all PCA, each ellipse represents the confidence intervals of the centroid position of the oocyte population. Two groups stand out: the first one is composed of cRhoA oocytes and prophase I oocytes (PI-Ctrl), and the second one is composed of cVCA oocytes, meiosis I and II oocytes. The first group clusters oocytes with thin actin cortices enriched in myosin-II (Figure 2A) and is associated with high cortical tension, high elastic modulus, and low capillary indentation ratio. In contrast, the second group clusters oocytes with thick actin cortices with fewer myosin-II (Figure 2A) and is associated with low cortical tension, low elastic modulus, and high capillary indentation ratio.

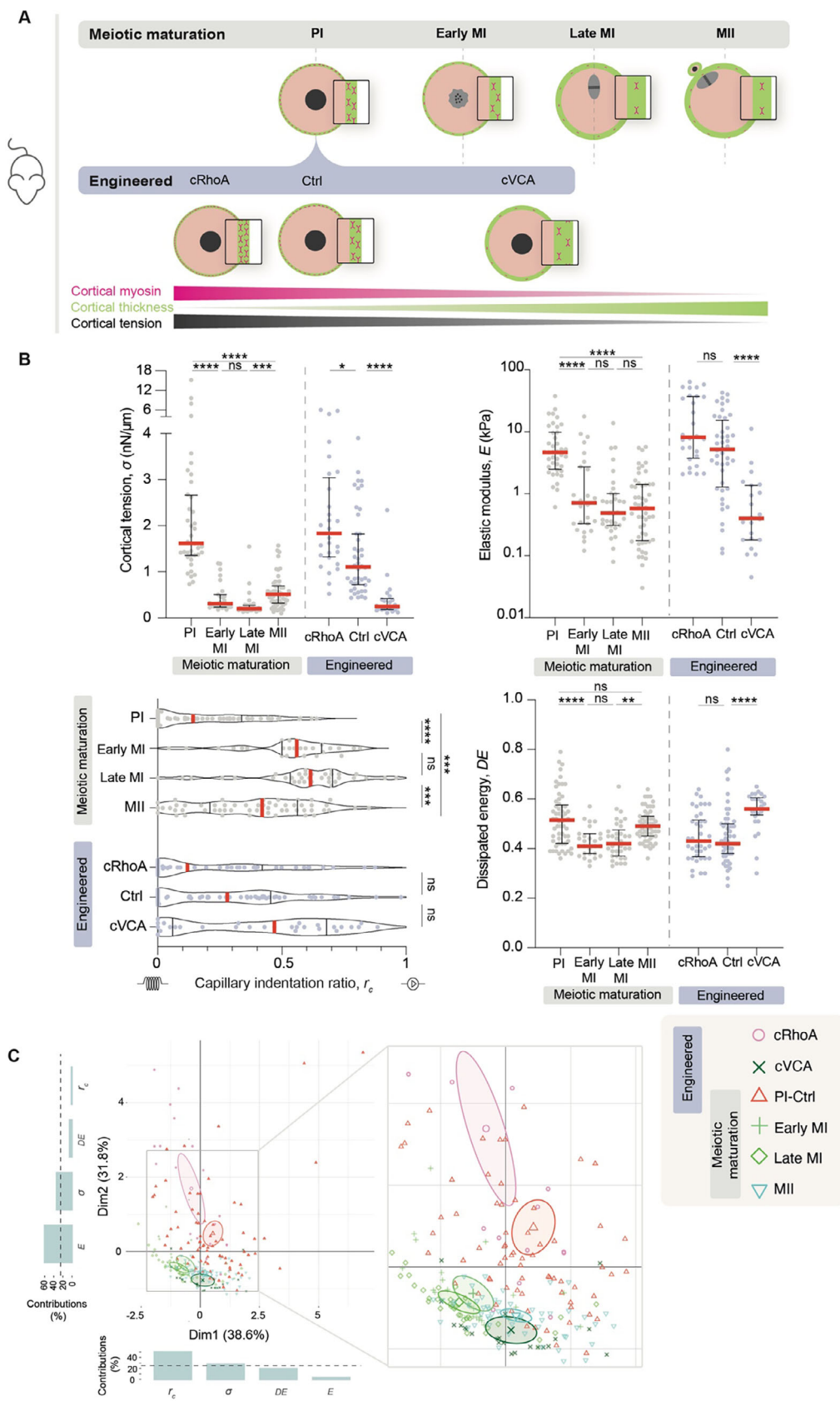
Our results highlight the tight relationship between cortex organization and mechanics. They suggest that oocyte mechanics could allow for inferring cortex organization.

## 2.3. Maternal Age Impacts Oocyte Mechanics and is Associated with a Modified Cortex organization

Maternal age is a well-known factor affecting the ability of an oocyte to develop into a proper embryo<sup>[37–39]</sup> but its effect on oocyte mechanics is unknown. We compared oocytes in prophase I obtained from young and aged female mice (11 and 44–56 weeks, respectively). We found that cortical tension and elastic modulus decrease with age ( $1.6 \text{ nN}\cdot\mu\text{m}^{-1}$  and  $9 \text{ kPa}$  for Young vs.  $1.0 \text{ nN}\cdot\mu\text{m}^{-1}$  and  $3 \text{ kPa}$  for Aged, Figure 3A), whereas capillary indentation ratio increases and normalized dissipated energy is constant. In PCA, oocytes from aged mice are located between the groups of oocytes with a thin actin cortex rich in myosin-II (cRhoA, PI-Ctrl and Young) and actin with a thick cortex and few myosin-II (meiosis I and cVCA) (Figure 3B).

We thus hypothesized that the cortex of oocytes in prophase I from aged mice resembles that of cVCA or meiosis I oocytes. To test this hypothesis, we characterized the actin cortex of oocytes from young and aged mice. Indeed, oocytes from old mice present a thicker cortex than oocytes from young mice (Figure 3C), as for oocytes in late meiosis I (Figure S3A, Supporting Information)<sup>[7]</sup> or cVCA oocytes.<sup>[7,11]</sup> Furthermore, we found that cortical actin fluorescence intensity is lower in oocytes from aged mice (Figure 3C), suggesting a different actin organization. We confirmed this hypothesis by measuring a higher cortical coherency<sup>[40,41]</sup> (see Materials and Methods) in these oocytes compared to those from young mice (Figure 3D, Figure S3B, Supporting Information).

Our results show that maternal age impacts oocyte mechanics: oocytes from aged mice are softer than those from young ones and harbor a differently organized and thicker actin cortex, further suggesting that oocyte mechanics reflect cortex organization.



## 2.4. Human and Mouse Oocyte Mechanics Diverge, Reflecting Differences in Cortex Organization

We then adapted our AFM measurement and analysis pipeline to human oocytes, whose mechanics and cortex organization during meiotic maturation are unknown. In mouse oocytes, cortical actin thickening and tension decrease between prophase I and meiosis I are key events for successful oocyte division.<sup>[7,11]</sup> We therefore studied human oocytes in prophase I (PI), meiosis I (MI), and meiosis II (MII) to determine whether similar processes regulate their division.

The cortical tension of mouse and human oocytes is of a similar order of magnitude, albeit lower for human oocytes (Figure 4A). However, and contrary to mouse oocytes, cortical tension in human oocytes is similar in prophase I and meiosis I (Figure 4A,  $0.6 \text{ nN}\cdot\mu\text{m}^{-1}$  for PI and MI), decreasing only in meiosis II (Figure 4A,  $0.3 \text{ nN}\cdot\mu\text{m}^{-1}$  for MII). The elastic modulus of human oocytes does not exhibit significant changes across the three stages; the capillary indentation ratio increases in meiosis II, and the normalized dissipated energy increases progressively during meiotic maturation (Figure 4A). We performed a PCA including human and mouse oocytes (Figure 4B). Human oocytes in prophase I and meiosis I overlap and are distinct from human oocytes in meiosis II. These three ellipses are close to those of the cVCA mouse oocytes.

The mechanical measurements and the PCA suggested potential differences in the organization of the human oocyte cortex compared to the mouse one. At the prophase I stage, human oocytes appear softer than mouse ones, suggesting that they could have a thicker actin cortex. The characterization of their actin cortex indeed revealed a thicker cortex for human compared to mouse oocytes in prophase I (Figures 3C and 4C). Furthermore, human oocytes in prophase I and meiosis I displayed the same mechanical parameters, suggesting an absence of cortical actin thickening after meiosis I entry in human oocytes, as is normally the case in mouse oocytes.<sup>[7]</sup> Indeed, our results show that human oocytes in prophase I and meiosis I present similar cortex thickness and cortical coherency (Figure 4C,D), with an actin density lower in meiosis I compared to prophase I (Figure 4C).

Therefore, as in mouse oocytes, variations in cortex structure correlate with the mechanical properties of human oocytes. However, the evolution of mechanical properties during meiotic maturation differs between human and mouse oocytes, the mechan-

ical profile changing later during meiotic maturation in human compared to mouse oocytes.

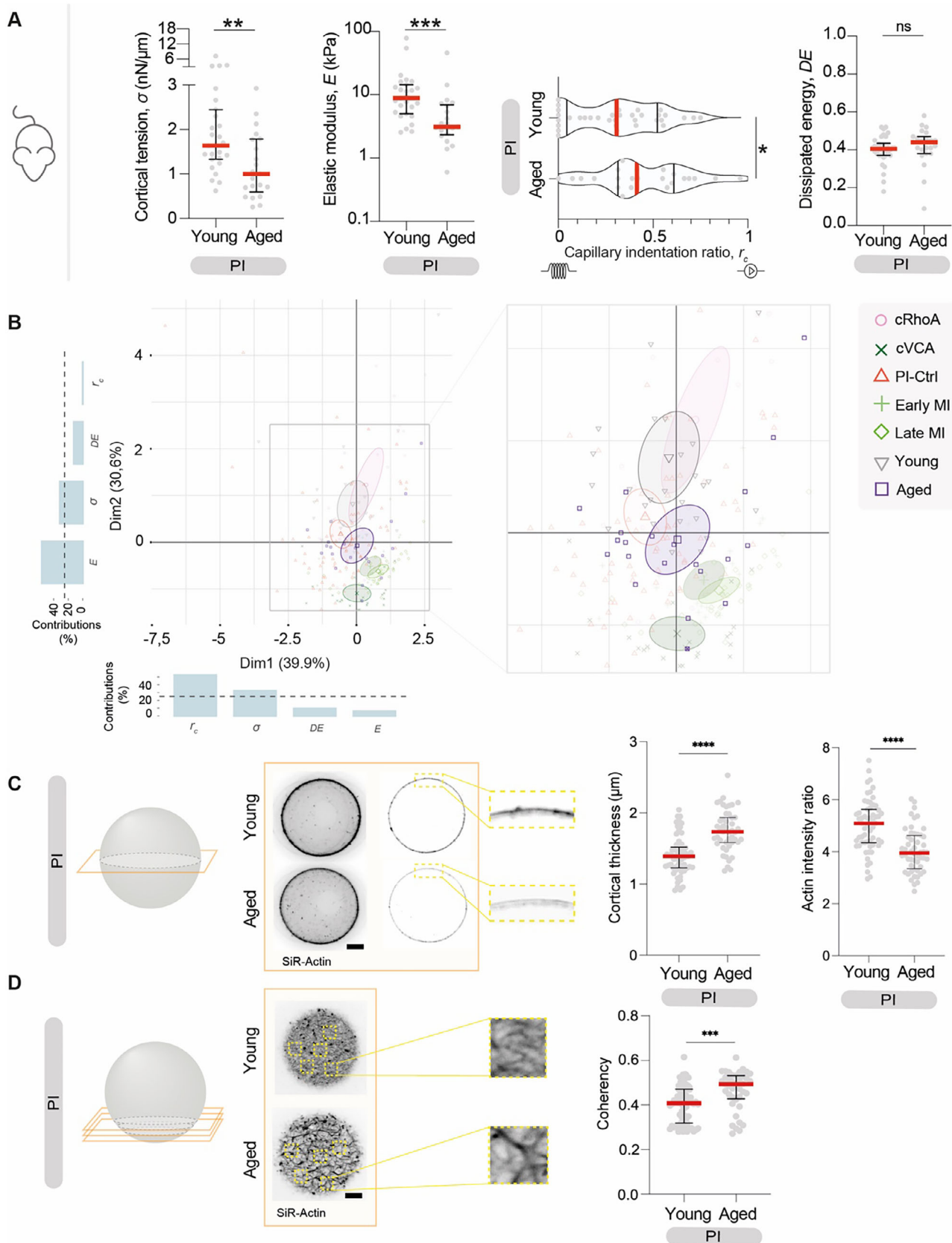
## 3. Discussion

In this study, we linked oocyte's mechanical properties to their actin cortical organization using AFM experiments: a thin actin cortex corresponds to stiff oocytes while a thick actin cortex is associated with softer oocytes. We also described this link between actin cortical organization and mechanical properties in the subfertile case of mouse advanced maternal age and in human oocytes.

We developed an elasto-capillary model to mechanically characterize oocytes probed with a local deformation. This model considers the deformation of a capillary element coupled to an elastic element. While the cell elastic modulus has been extensively investigated at the local scale in numerous AFM studies,<sup>[26,27,30]</sup> capillary deformation has been considered only at the scale of the oocyte's global deformation.<sup>[42]</sup> Furthermore, previous research suggested that both elastic and capillary response should be considered, especially in cases involving local deformations, as in our study.<sup>[23,24]</sup> Indeed, we found that our model better describes the oocyte's response to a small indentation than models that take into account only one of these non-dissipative responses. Our model could be applied to other cell types as cancer cells, which have so far been mainly characterized using elastic models in AFM.<sup>[12]</sup> More refined models could be useful in the future, as models taking into account the cortex viscoelasticity<sup>[23,35]</sup> instead of only the dissipation, but it would require the analysis of the cell shape during indentation.

Our AFM measurements resulted in four mechanical parameters from a single oocyte measurement. We combined them using a PCA, to visualize the mechanical phenotypes of each oocyte population studied. This analysis allowed to discriminate between groups that were indistinguishable using a single parameter. For example, cVCA and late meiosis I oocytes have the same cortical tension but appear separate on the PCA. Interestingly, a previous study has combined several mechanical parameters to identify mammalian early embryos with the best developmental potential.<sup>[9]</sup> In another study, the clustering and discrimination of metastatic cancer cells were improved by integrating mechanical data with genetic and morphological data.<sup>[43]</sup>

**Figure 2.** Oocyte mechanics predict cortex organization. A) Scheme of the different oocytes with known cortical organization and known cortical tension measured with AFM, displaying cortex organization (cortical thickness in green, cortical myosin-II in pink). The upper row shows oocytes at different stages of meiotic maturation (prophase I: PI, early meiosis I: early MI, late meiosis I: late MI, meiosis II: MII). The middle row shows engineered oocytes in prophase I with a modified cortex (cVCA, cRhoA), with their control (Ctrl) expressing only a cortical anchor. The lower row shows the enrichment of actin (cortical thickness in green) and myosin-II (cortical myosin-II in pink) in the cortex of the oocytes displayed above, along with their cortical tension (measured previously with micropipette aspiration). The nucleus is shown as a black circle, the microtubule spindle as a gray oval, and the chromosomes as black circles (after meiosis I entry). B) Evolution of mechanical parameters during meiotic maturation (PI, early MI, late MI, MII) and for engineered oocytes (cRhoA, cVCA, Ctrl) in prophase I. Graphs showing cortical tension  $\sigma$  ( $\text{nN}\cdot\mu\text{m}^{-1}$ ), elastic modulus  $E$  (kPa), capillary indentation ratio  $r_c$ , and dissipated viscous energy  $DE$ . Data are medians and quartiles with individual data points plotted from at least three experiments. For cortical tension and elastic modulus, 40 PI, 27 early MI, 33 late MI, 53 MII, 28 cRhoA, 44 Ctrl, and 22 cVCA were measured. For capillary indentation ratio, 58 PI, 27 early MI, 34 late MI, 57 MII, 42 cRhoA, 58 Ctrl, and 29 cVCA were measured. For the normalized dissipated viscous energy, 58 PI, 27 early MI, 34 late MI, 57 MII, 42 cRhoA, 57 Ctrl, and 29 cVCA were measured. The statistical significance was assessed by an ANOVA test or a Kruskal-Wallis test with Tukey or Dunn multiple comparisons test, respectively, depending on whether the data followed a Gaussian distribution. In all graphs, ns corresponds to not significant, \* corresponds to a  $P$ -value  $< 0.05$ , \*\* to a  $P$ -value  $< 0.01$ , \*\*\* to a  $P$ -value  $< 0.001$  and \*\*\*\* to a  $P$ -value  $< 0.0001$ . C) Principal component analysis of the four mechanical parameters for the different stages of meiotic maturation and engineered oocytes (20 cRhoA, 77 PI-Ctrl, 22 cVCA, 27 early MI, 33 late MI, and 53 MII). The graphs show the percentage contributions of the four mechanical parameters in PCA Dimension 1 (Dim-1) and Dimension 2 (Dim-2). The black dotted line is 25%.



Ultimately, mechanical measurements of oocytes could be added to the current multiparametric approach used to identify pathological oocytes in assisted reproductive technology.<sup>[44]</sup>

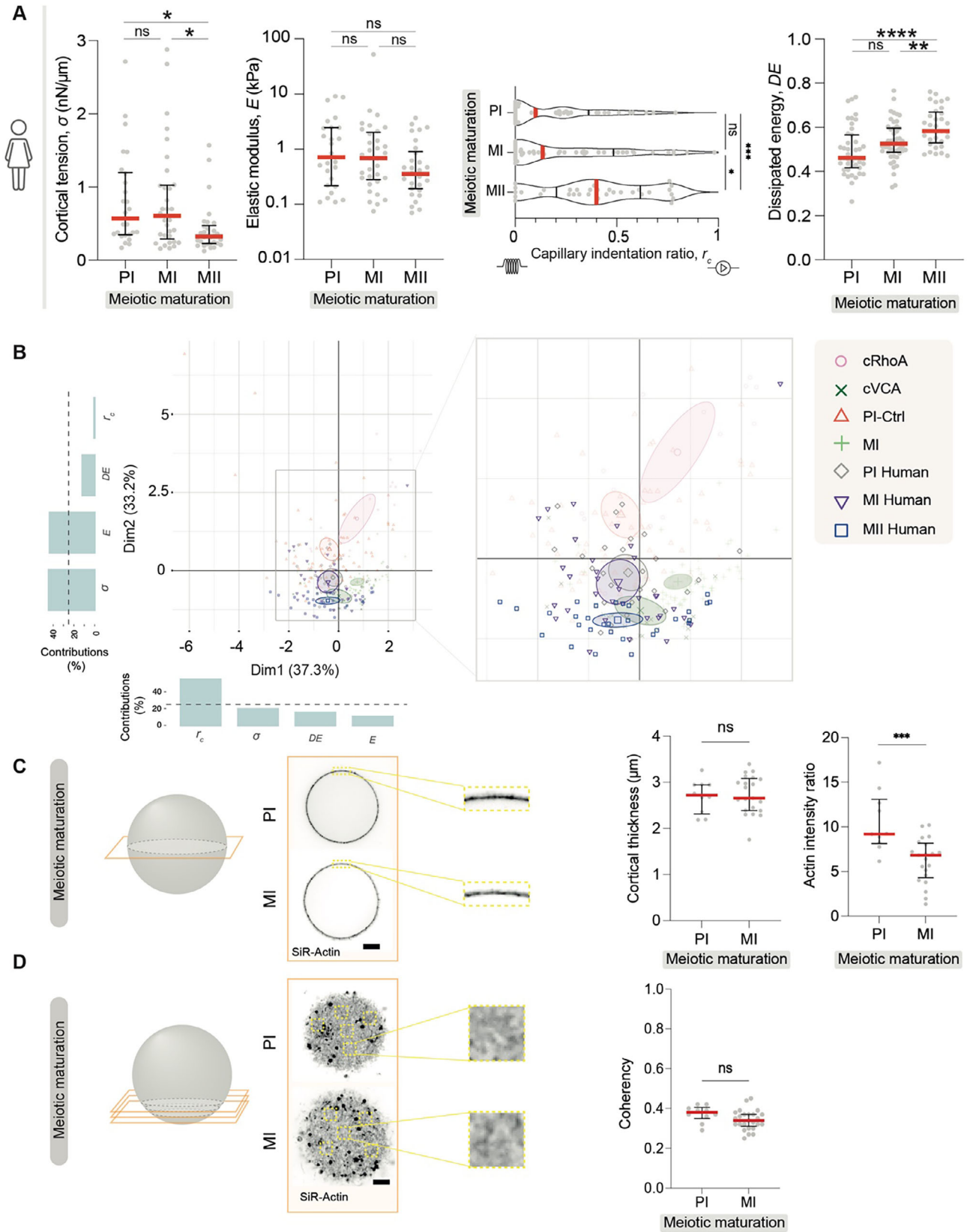
Focusing on the impact of maternal age, we show that oocytes from old mice are softer than those from young ones with a differently organized actin cortex. A previous study<sup>[45]</sup> using a different technique showed that oocytes arrested in meiosis II with their *Zona Pellucida* exhibited significantly lower elastic modulus when retrieved from aged mice compared to young ones (3.1 vs. 1.6 kPa, respectively), which is in agreement with our results. We show that the cortex of oocytes from aged mice is thicker but less dense than that of oocytes from young mice, suggesting that the cortical actin quantity might be similar or lower in oocytes from aged mice compared to young ones. These results are in agreement with those of a previous study that reported a lower amount of F-actin in aged mice, especially in a sub-cortical region.<sup>[46]</sup> Moreover, coherency analysis shows that cortical actin organization differs significantly between oocytes from young and old mice. These differences could be due to the influence of aging on proteins, including cytoskeletal components.<sup>[39]</sup> Interestingly, it has been shown that cortex softening induces aneuploidy, meaning an abnormal number of chromosomes.<sup>[10]</sup> Therefore, the softening of oocytes associated with maternal age could contribute to the increased aneuploidy rates observed in oocytes from older mammals.<sup>[39]</sup> Investigating the molecular mechanisms underlying these changes in cortex organization would be of great interest.

We probed human oocytes and showed that their mechanical properties evolve differently compared to those of mouse oocytes during meiotic maturation. Cortical tension does not decrease after meiosis I entry in human oocytes, but only in meiosis II. Similarly, their capillary indentation ratio only increases in meiosis II, reflecting a delayed transition from an elastic behavior to a capillary-dominated response. There is a gradual increase in normalized dissipated energy during meiotic maturation, but no significant changes in elastic modulus. One study found that elastic modulus increases between MI and MII in human oocytes, measured by AFM.<sup>[26]</sup> However, these measurements were performed with the *Zona Pellucida*. Another study analyzed the characteristics of the human oocyte cytoplasm

through the persistence of the injection funnel after intracytoplasmic sperm injection,<sup>[47]</sup> showing that human oocyte viscosity increases from prophase I to meiosis II, which is consistent with our results. We show that the differences in mechanics measured between mouse and human oocytes are associated with distinct cortical organizations, as highlighted by the absence of cortical actin thickening in human oocytes after entry in meiosis I. In mouse oocytes, the decrease of cortical tension in meiosis I due to cortical actin thickening is essential for the asymmetry in size of the first meiotic division.<sup>[7,10,11]</sup> Human oocytes also divide asymmetrically. However, the lack of cortical actin thickening suggests that alternative mechanisms or cytoskeleton structures may be involved in regulating human oocyte geometry of division.

Finally, this work demonstrates that a thin actin cortex enriched in myosin-II corresponds to stiff oocytes with high cortical tension and elastic modulus. In contrast, a thick actin cortex with less myosin-II is associated with lower cortical tension and elastic modulus. These findings suggest specific links between cortical organization and mechanics in mouse and human oocytes, raising questions about the underlying regulatory mechanisms. In vitro studies have shown that actin density and cross-linking control the elasticity of actin networks.<sup>[48]</sup> In vivo, altering the orientation of actin filaments, such as transitioning from an actin mesh to fibers, decreases connectivity and affects cell effective elasticity.<sup>[40,41]</sup> In our case, the oocyte cortex and the cortical thickening are nucleated by different actin nucleators and are therefore made up of a different actin architecture.<sup>[7,49]</sup> Interestingly, it was shown in fibroblasts that the cortex encloses regions of low (“mesh”), intermediate (“mixed”), and high (“fibers”) coherency. These different values of coherency correlate with local mechanical properties: regions with low coherency have the highest rigidity.<sup>[40,41]</sup> Accordingly, this is also what we observe in the case of oocytes from aged mice. Actin dynamics and motor activity control cell tension,<sup>[6]</sup> in agreement with in vitro works showing that myosin motors and the organization of actin filaments influence network tension.<sup>[50]</sup> Besides, increasing myosin penetration into the actin cortex results in a thinner cortex and higher cortical tension.<sup>[51]</sup> Therefore, there is generally a subtle crosstalk between actin network structure, dynamics and crosslinking, and

**Figure 3.** Maternal age impacts oocyte mechanics and is associated with a modified cortex organization. A) Graphs showing the mechanical parameters (cortical tension  $\sigma$  (nN. $\mu\text{m}^{-1}$ ), elastic modulus  $E$  (kPa), capillary indentation ratio  $r_c$ , and normalized dissipated viscous energy  $DE$  for prophase I (PI) oocytes coming from Young (11-week-old) and Aged (44-56-week-old) mice. Data are medians and quartiles with individual data points plotted from three independent experiments. For cortical tension and elastic modulus, 27 oocytes from Young mice and 22 from Aged mice were analyzed. For capillary indentation ratio and normalized dissipated viscous energy, 34 oocytes from Young mice and 23 from Aged mice were analyzed. The statistical significance of differences between 2 groups was assessed with an unpaired t-test or a nonparametric Mann-Whitney test, depending on whether the data followed a Gaussian distribution. In all graphs, ns corresponds to not significant, \* to a  $P$ -value < 0.05, \*\* to a  $P$ -value < 0.01, and \*\*\* to a  $P$ -value < 0.001. B) Principal component analysis of the four mechanical parameters for different stages of meiotic maturation, engineered oocytes, and oocytes coming from Young and Aged mice (20 cRhoA, 77 PI-Ctrl, 22 cVCA, 27 early MI, 33 late MI, and 53 MII, 27 Young and 22 Aged). Ellipses indicate 95% confidence intervals. The graphs show the percentage contribution of the four mechanical parameters in PCA Dimension 1 (Dim-1) and Dimension 2 (Dim-2). The black dotted line is set at 25%. C) Confocal spinning disc images of prophase I (PI) oocytes coming from Young (11-week-old) and Aged (44-56-week-old) mice stained with SiR-Actin (black). Scale bar: 5  $\mu\text{m}$ . One Z plane is shown. Graph showing the cortical thickness and the actin fluorescence ratio between the cortex and the cytoplasm of 47 prophase I (PI) oocytes coming from Young (11-week-old) and 59 prophase I (PI) oocytes coming from Aged (44-56-week-old) mice. Data are medians and quartiles with individual data points plotted from three independent experiments. The statistical significance of differences between 2 groups was assessed with a nonparametric Mann-Whitney test. In all graphs, \*\*\*\* corresponds to a  $P$ -value < 0.0001. D) Confocal spinning disc images of prophase I (PI) oocytes coming from Young (11-week-old) and Aged (44-56-week-old) mice stained with SiR-Actin (black). Scale bar: 10  $\mu\text{m}$ . A projection of five Z planes is shown. Graph showing the coherency of cortex actin network calculated in 5.33  $\mu\text{m}^2$  square ROIs for 67 prophase I (PI) oocytes coming from Young (11-week-old) and 40 prophase I (PI) oocytes coming from Aged (44-56-week-old) mice. Data are medians and quartiles with individual data points plotted from two independent experiments. The statistical significance of differences between 2 groups was assessed with an unpaired t-test. In the graph, \*\*\*\* corresponds to a  $P$ -value < 0.001.



motor activity, which we clearly highlight in our experiments. Moreover, some effects could be redundant. For instance, myosin is a motor and a crosslinker, which may explain why tension and elasticity follow the same trend in mouse oocytes. Deciphering these different aspects further would provide a better understanding of how the different mechanical properties of oocytes are regulated and connected.

#### 4. Experimental Section

**AFM-Indentation Measurements:** Oocytes without their *Zona Pellucida* were measured to study the mechanical properties of the oocyte cortex. Cells were immobilized with an electronic microscopy hexagonal nickel grid (Ref. DT300H-Ni,  $\varnothing$  3.05 mm, thickness 18  $\mu\text{m}$ , hole 73  $\mu\text{m}$ ; Gilder) attached to the surface of a petri dish filled with medium.<sup>[32]</sup> Note that the oocytes were immobilized, but not blocked or confined in the grid to avoid any effect on the mechanical measurement (Figure S1A–C, Supporting Information). AFM indentation measurements were performed on a Nanowizard IV AFM (Bruker - JPK Instruments) coupled to a widefield microscope (Zeiss Axio Observer with Hamamatsu sCMOS Flash 4.0 Camera) in contact mode. MLCT-C tips (Bruker, with silicon nitride cantilevers; nominal spring constant = 0.01  $\text{N}\cdot\text{m}^{-1}$ ) with a 17° side angle, a 5- $\mu\text{m}$  average height pyramidal tip, and a 20-nm tip radius were used. The calibration of the MLCT cantilevers was performed as follows: the sensitivity of the cantilever deflection was determined by collecting a force curve on the stiff surface of a Petri dish filled with milli-Q water<sup>[52]</sup> and was analyzed by the JPK processing software. The cantilever's spring constant was obtained using the thermal tune method.<sup>[53]</sup> Ten force curves were acquired for each oocyte at the same position with a 1  $\mu\text{m}\cdot\text{s}^{-1}$  approach velocity and a 0.5 nN set point (Figure S1D–F, Supporting Information). The measurement takes no more than 1 min for each oocyte. Importantly, there were low variations between repeated indentations and in the mechanical parameters extracted for the same oocyte (Figure S1D–F, Supporting Information), showing that our measurement was quite robust and reproducible and that the oocyte mechanical response was stable during the measurements, as there was no trend in the mechanical parameters measured throughout the indentations (no local stiffening/softening due to the repeated AFM indentations).

Force distance curves were converted into force-indentation curves with JPK processing software (version 6.1) by subtracting the cantilever bending from the piezo height to get the accurate vertical tip position. First, the contact point was roughly determined using the JPK software, which performs a linear regression on the force baseline and a linear fitting of the beginning of the force curve, placing the contact point at the intersection of these two lines. Then, a R code was written, which varies

the x-position of the contact point within a window of values A (–0.5 to 0.5  $\mu\text{m}$  around the contact point given by the JPK software). For each contact point value, the curve was fit with the model combining elasticity and surface tension (Equation (3)) with E and  $\sigma$  as free parameters, and initial values of these parameters of 10 kPa, a typical value for cell elasticity<sup>[54]</sup> and  $\text{1 nN}\cdot\mu\text{m}^{-1}$ , the tension obtained for oocytes by micropipette aspiration.<sup>[7]</sup> The Residual Standard Error (RSE) was calculated for each fit. The contact point value was retrieved, corresponding to the minimum RSE in window A; a new, smaller window of values B (–0.2 to 0.2  $\mu\text{m}$  around the contact point) was defined, and the fitting sequence was repeated. In total, 5 steps of “zooming” around the contact point was used to get the lower value of the RSE and thus accurately determine the contact point. Finally, cortical tension  $\sigma$  and elastic modulus E were extracted in this optimized contact point position and used to calculate the capillary indentation ratio parameter  $r_c$  (Equation (4)). Then, the median of cortical tension  $\sigma$ , elastic modulus E, and capillary indentation ratio  $r_c$  was calculated for each oocyte with a minimum of five measurements. The curve fitting and determination of the contact point were done with R Studio software (version 2022.12.0+353). The R code is accessible at <https://doi.org/10.5281/zenodo.14999026>. The median and the calculation of the quartiles were done with GraphPad Prism 9.5.0 for MacOS, GraphPad Software, La Jolla, CA, USA (version 9.5.0 (525)).

The viscous dissipated energy was calculated by trapezoidal integration of the area between the approach and retraction curves for the positive-indentation region. The value was normalized by the area under the approach curve. All these analyses were done using R Studio software (version 2022.12.0+353).

Finally, for each oocyte, the median of normalized viscous energy was calculated with a minimum of five measurements with GraphPad Prism 9.5.0 for MacOS, GraphPad Software, La Jolla, CA, USA (version 9.5.0 (525)).

**Mouse Oocyte Collection and Culture:** Ovaries were collected from 11-week-old and 44–56-week-old OF1 female mice. Fully-grown oocytes in prophase I (PI) were extracted by shredding the ovaries in homemade M2 medium<sup>[55]</sup> supplemented with milrinone (1  $\mu\text{m}$ )<sup>[56]</sup> or dibutyryl cyclic AMP (dbcAMP) (0.1  $\text{mg mL}^{-1}$ )<sup>[57]</sup> to maintain them in prophase I. The *Zona Pellucida* of PI oocytes was removed by incubating them in a homemade M2 medium supplemented with milrinone (1  $\mu\text{m}$ ) or dbcAMP (0.1  $\text{mg mL}^{-1}$ ) and 0.4% pronase.<sup>[58]</sup> Prophase I exit was triggered by releasing oocytes into a homemade M2 medium. All live culture and imaging were carried out under oil at 37°C.

**Ethical Statement:** All animal studies were performed in accordance with the guidelines of the European Community and were approved by the French Ministry of Agriculture (authorization D750512).

**Human Oocyte Collection and Culture:** The use of human oocytes not arrested in meiosis II and therefore not usable for patients has been approved by the local ethics committee of the Hospices Civils de Lyon (agreement number 22\_5725). All patients gave informed consent.

**Figure 4.** Human and mouse oocyte mechanics diverge, reflecting differences in cortex organization. A) Graphs showing the mechanical parameters (cortical tension  $\sigma$  ( $\text{nN}\cdot\mu\text{m}^{-1}$ ), elastic modulus E (kPa), capillary indentation ratio  $r_c$ , and normalized dissipated viscous energy DE for different stages of human oocyte meiotic maturation (prophase I (PI), meiosis I (MI) and meiosis II (MII)). Data are medians and quartiles with individual data points plotted from four independent experiments. For cortical tension and elastic modulus, 26 PI, 33 MI, and 30 MII were analyzed. For capillary indentation ratio and normalized dissipated viscous energy, 43 PI, 47 MI, and 33 MII were analyzed. The statistical significance was assessed by an ANOVA test or a Kruskal-Wallis test with Tukey or Dunn multiple comparisons test, respectively, depending on whether the data followed a Gaussian distribution. In all graphs, ns corresponds to not significant, \* corresponds to a  $P$ -value < 0.05, \*\* to a  $P$ -value < 0.01, and \*\*\*\* to a  $P$ -value < 0.0001. B) Principal component analysis of the four mechanical parameters for different stages of mouse oocyte meiotic maturation and engineered mouse oocytes and the different stages of human oocytes meiotic maturation (20 cRhoA, 77 PI-Ctrl, 22 cVCA, 50 MI, 26 human PI, 33 human MI, and 30 human MII). Ellipses indicate 95% confidence intervals. The graphs show the percentage contribution of the four mechanical parameters in PCA Dimension 1 (Dim-1) and Dimension 2 (Dim-2). The black dotted line is set at 25%. C) Confocal spinning disc images of human oocytes stained with SiR-Actin (black) in prophase I (PI) and meiosis I (MI). One Z plane is shown. Scale bar: 20  $\mu\text{m}$ . Graph showing the cortical thickness and the actin fluorescence ratio between the cortex and the cytoplasm of 10 PI and 21 MI human oocytes. Data are medians and quartiles with individual data points plotted from three independent experiments. Statistical significance of differences between 2 groups was assessed with a parametric t-test. In all graphs, ns corresponds to not significant and \*\*\*\* to a  $P$ -value < 0.001. D) Confocal spinning disc images of human oocytes stained with SiR-Actin (black) in prophase I (PI) and meiosis I (MI). A projection of six Z planes is shown. Scale bar: 10  $\mu\text{m}$ . Graph showing the coherency of the actin network calculated in 5.33  $\mu\text{m}$  square ROIs of 10 PI and 25 MI oocytes. Data are medians and quartiles with individual data points plotted from three independent experiments. Statistical significance of differences between 2 groups was assessed with a parametric t-test. In the graph, ns corresponds to not significant.

Patients undergoing Assisted Reproductive Technologies (ART) for intracytoplasmic sperm injection (ICSI) had multi-follicular ovarian stimulation. When the ovarian follicles were mature, patients underwent follicular fluid puncture to recover the cumulo-oocyte complexes (COCs). The follicular fluid was screened, and the COCs were cultured in media (Sequential Fert, Origio, Denmark) under oil (Liquid Paraffin, Origio, Denmark) at 37°C, 5% CO<sub>2</sub>, and 5% O<sub>2</sub> in an incubator during 1 h, and then enzymatically (80 U mL<sup>-1</sup> recombinant human hyaluronidase, ICSI Cumulase, Origio) and mechanically denuded. The denuded oocytes were observed under the light microscope to determine their stage. Only oocytes arrested in meiosis II were used for ICSI. The other oocytes in prophase I or meiosis I were unsuitable for ICSI and were used in this study.

The *Zona Pellucida* of human oocytes was removed by incubating them into sequential Fert (Origio, Denmark) with tyrod acid (T1788, Sigma-Aldrich, USA) for 3 s. The oocytes were rinsed in sequential Fert and cultured in media (Sequential Fert, Origio, Denmark) under oil (Liquid Paraffin, Origio, Denmark) at 37°C, 5% CO<sub>2</sub>, and 5% O<sub>2</sub> in an incubator.

Meiosis II oocytes were obtained from prophase I or meiosis I oocytes matured in vitro for up to 24 h in a specific medium (MediCult IVM, Origio) supplemented with Follicle Stimulating Hormone (FSH) 75 mIU (Bemfola, GedeonRichter, Hungary), Human chorionic gonadotropin (hCG) (Ovitrelle, Merck, Germany) and Serum Substitute Supplement (SSS) 10% (FujiFilm Irvine Scientific, USA). Oocytes were incubated at 37°C in a controlled atmosphere of 5% CO<sub>2</sub> and 5% O<sub>2</sub>.

**In Vitro Transcription of cRNAs and Mouse Oocytes Microinjection:** The following constructs were used: pRN3-EzTD-mCherry-RhoA<sup>[36]</sup> (cRhoA), gift from Rong Li (Mechanobiology Institute, Singapore), pRN3-EzTD-mCherry<sup>[59]</sup> (Ctrl), and pRN3-EzTD-mCherry-VCA<sup>[11]</sup> (cVCA).

Plasmids were linearized using appropriate restriction enzymes. cRNAs were synthesized with the mMessage mMachine kit (Ambion) and subsequently purified using the RNeasy kit (Qiagen) following the manufacturer's instructions.<sup>[60]</sup> Their concentration was measured using NanoDrop 2000 from ThermoScientific. Their final concentrations were >800 ng.μL<sup>-1</sup>. cRNAs were centrifuged at 4°C for 45 min at 20 000g prior to microinjection into the cytoplasm of oocytes blocked in prophase I in homemade M2 medium supplemented with 1 μM milrinone or 0.1 mg mL<sup>-1</sup> dbcAMP at 37°C, using an Eppendorf Femtojet micro-injector.<sup>[61]</sup> After microinjection, cRNA translation was allowed for 4h to allow direct comparison with cortical tension measurements made with micropipette aspiration on oocytes, where translation was allowed for 4h.<sup>[11]</sup>

**Fluorescent Probes for Live Imaging:** Mouse and human oocytes were incubated for 30 min in homemade M2 medium and Fertmedium respectively supplemented with SiR-actin (1 μM) (Spirochrome- SiR-actin Kit (SC001)) and Hoechst (5 ng.mL<sup>-1</sup>) (Sigma-Aldrich H6024) to label F-actin and DNA. For mouse oocytes, immediately after incubation, spinning disk images were acquired using a Plan-APO x40/1.25NA objective on a Leica DMI6000B microscope enclosed in a thermostatic chamber (Life Imaging Service) equipped with a Retiga 3 CCD camera (QImaging) coupled to a Sutter filter wheel (Roper Scientific) and a Yokogawa CSU-X1 Spinning disk. For human oocytes, spinning disk images were acquired using an HCX PL APO x40 and x63 objectives on a Leica DMI4000 microscope with a confocal system CSU-W1-T1 Yokogawa enclosed in a thermostatic chamber equipped with a Photometrics PRIME 95B camera. Metamorph software (Universal Imaging) was used to collect data, and ImageJ (NIH) was used to analyze and process data.

**Cortical Thickness and Fluorescent Measurements:** Cortical thickness was measured in oocytes incubated with SiR-Actin on a Z-slice going through the widest part of the oocyte to avoid projection artifacts. Thickness was measured by manually placing lines perpendicularly to the cortex in at least four different oocyte cortex regions. The average of these measurements was the cortical thickness of a given oocyte multiplied by the pixel size.

The actin fluorescence ratio was measured manually by measuring the ratio between the mean of the fluorescence signal at the cortex and in the cytoplasm.

**Coherency Measurement:** The coherency quantifies the degree of anisotropy in an image with values ranging from 0 (isotropic, no preferred

orientation) to 1 (highly anisotropic, strong directional preference), as previously used to quantify the organization of the actin cortex.<sup>[40,41]</sup> This method does not depend on intensity nor requires image thresholding.

Cortical actin network coherency was measured in oocytes incubated with SiR-Actin on the first five cortical z-slices separated by 1 μm and projected together, taking the maximum signal intensity to image the surface of the cortex and have a better view of its organization.<sup>[49]</sup> Coherency was measured in at least 5 square ROIs of 5.33 μm in length and at least 2 square ROIs of 10.6 μm in length using the Orientation Analysis plugin in ImageJ (version 2.14.0/1.54f). The average of these measurements was the cortical coherency of a given oocyte.

**Statistical Analysis:** The statistical analysis was performed using GraphPad Prism 9.5.0 for MacOS, GraphPad Software, La Jolla, CA, USA (version 9.5.0 (525)). For comparison between two groups, the normality of the values was tested using a D'Agostino-Pearson's normality test. The statistical significance of differences was assessed by an unpaired t-test (for a normal distribution of the values) or by a nonparametric Mann-Whitney test (for values that did not follow a normal distribution). For comparison of more than two groups, the statistical significance was assessed by an ANOVA test or a Kruskal-Wallis test with Tukey or Dunn multiple comparisons test, respectively, depending on whether the data followed a Gaussian distribution. All tests were performed with a confidence interval of 95%. Data were medians and quartiles with individual data points plotted from at least two independent experiments. The sample size (n) for each statistical analysis was indicated in the figure's legends. In all graphs, ns corresponds to not significant, \* corresponds to a P-value<0.05, \*\* to a P-value<0.01, \*\*\* to a P-value<0.001, and \*\*\*\* to a P-value<0.0001.

**Principal Component Analysis:** PCA analysis was performed to facilitate the visualization of our multiparametric dataset and to potentially identify oocyte populations belonging to the same groups based on their mechanical properties. This approach helps to reduce the dimensionality of the dataset. PCA transforms the original dataset into a new set of uncorrelated principal components (PCs), ordered by the amount of variance they capture. The first few PCs typically explain most of the variability in the data, enabling meaningful data representation in a lower-dimensional space. Each mechanical parameter was first standardized by subtracting the mean and dividing by the standard deviation of its population to ensure all parameters contribute equally to the PCA. The correlation between mechanical parameters was assessed, ensuring that no pair of parameters had a correlation coefficient higher than 0.75, to avoid redundancy. Finally, the principal component analysis test was run with the PCA function from the FactoMineR<sup>[62]</sup> R package. Associated plots were generated with the factoextra<sup>[63]</sup> R package. On the PCA graph, each point corresponds to the scaled median of all measures for each mechanical parameter per oocyte. To better visualize each oocyte population, 95% confidence ellipses of the centroid positions of each population were displayed. Non-overlapping 95% confidence ellipses suggested a statistically significant difference between groups.

## Supporting Information

Supporting Information is available from the Wiley Online Library or from the author.

## Acknowledgements

The authors thank all members of the Verlhac-Terret and LAMBE labs for discussions, the CIRB animal facility, Tristan Piolot from the Orion facility, Fanny Sibaud for her role in the initiation of this project, and all the members of the LYMIC-PLATIM, especially Simoné Bovio and Elodie Chatre, for all their advices and discussions. The AFM microscopy was performed at the Orion Platform (member of France-Bioimaging ANR-10-INBS-XX) of the Center for Interdisciplinary Research in Biology (UMR7241/U1050) of the Collège de France. The authors acknowledge the contribution of SFR Biosciences (Université Claude Bernard Lyon 1, CNRS UAR3444, Inserm

US8, ENS de Lyon) PLATIM-LyMIC, especially Simoné Bovio for assistance in AFM experiment and Elodie Chatre with live imaging experiment. This work was supported by DIM ELICIT du Conseil régional d'Ile de France (DIM ELICIT-AAP-2020 to MET), Biomedical Engineering seed grant program (BME to CC), PSL-QLife (Q-life ANR-17-CONV-0005 to MET), the ANR (ANR-24-CE13-5691 to MET) and FRM ECO- Contrat doctoral program (ECO202206015524 to RB). ML was supported by the Fondation Bettencourt-Schueller under the Impulscience program. This work has received support from the Fondation Bettencourt Schueller, support under the program « Investissements d'Avenir » launched by the French Government and implemented by the Agence Nationale de la Recherche, with the references: ANR-10-LABX-54 MEMO LIFE, ANR-11-IDEX-0001-02 PSL\* Research University.

## Conflict of Interest

The authors declare no conflict of interest.

## Author Contributions

R.B. and L.B. contributed equally to this work. CC and MET conceived the project that was directed by CC, MET and EL. MHV was involved in some aspects of project supervision. RB, LB, and YL designed, performed, and analyzed all experiments, with the help of GL for AFM. ML built the elasto-capillary model. NT did the PCA. RB wrote the manuscript, which was seen and corrected by all authors.

## Data Availability Statement

The data that support the findings of this study are available from the corresponding author upon reasonable request.

## Keywords

actomyosin cortex, atomic force microscopy, biomechanics, cortical tension, elastic modulus, oocytes

Received: June 1, 2025  
Revised: November 3, 2025  
Published online:

- [1] H. K. Matthews, U. Delabre, J. L. Rohn, J. Guck, P. Kunda, B. Baum, *Dev. Cell.* **2012**, *23*, 371.
- [2] M. Plodinec, M. Loparic, C. A. Monnier, E. C. Obermann, R. Zanetti-Dallenbach, P. Oertle, J. T. Hyotyla, U. Aebi, M. Bentires-Alj, R. Y. H. Lim, C.-A. Schoenenberger, *Nature Nanotech.* **2012**, *7*, 757.
- [3] M. Lekka, K. Pogoda, J. Gostek, O. Klymenko, S. Prauzner-Bechcicki, J. Wiltowska-Zuber, J. Jaczewska, J. Lekki, Z. Stachura, *Micron.* **2012**, *43*, 1259.
- [4] L. Blanchoin, R. Boujemaa-Paterski, C. Sykes, J. Plastino, *Physiol. Rev.* **2014**, *94*, 235.
- [5] E. Evans, A. Yeung, *Biophys. J.* **1989**, *56*, 151.
- [6] J.-Y. Tinevez, U. Schulze, G. Salbreux, J. Roensch, J.-F. Joanny, E. Paluch, *Proc. Natl. Acad. Sci. USA.* **2009**, *106*, 18581.
- [7] A. Chaigne, C. Campillo, N. S. Gov, R. Voituriez, J. Azoury, C. Umaña-Díaz, M. Almonacid, I. Queguiner, P. Nassoy, C. Sykes, M.-H. Verlhac, M.-E. Terret, *Nat. Cell Biol.* **2013**, *15*, 958.
- [8] S. M. Larson, H. J. Lee, P. Hung, L. M. Matthews, D. N. Robinson, J. P. Evans, *MBoC.* **2010**, *21*, 3182.
- [9] L. Z. Yanez, J. Han, B. B. Behr, R. A. R. Pera, D. B. Camarillo, *Nat. Commun.* **2016**, *7*, 10809.
- [10] I. Bennabi, F. Crozet, E. Nikalayevich, A. Chaigne, G. Letort, M. Manil-Ségalen, C. Campillo, C. Cadart, A. Othmani, R. Attia, A. Genovesio, M.-H. Verlhac, M.-E. Terret, *Nat. Commun.* **2020**, *11*, 1649.
- [11] A. Chaigne, C. Campillo, N. S. Gov, R. Voituriez, C. Sykes, M. H. Verlhac, M. E. Terret, *Nat. Commun.* **2015**, *6*, 6027.
- [12] M. Liboz, A. Allard, M. Malo, G. Lamour, G. Letort, B. Thiébot, S. Labdi, J. Pelta, C. Campillo, *ACS Appl. Mater. Interfaces.* **2023**, *15*, 43403.
- [13] R. Vargas-Pinto, H. Gong, A. Vahabikashi, M. Johnson, *Biophys. J.* **2013**, *105*, 300.
- [14] L. Ramms, G. Fabris, R. Windoffer, N. Schwarz, R. Springer, C. Zhou, J. Lazar, S. Stiefel, N. Hersch, U. Schnakenberg, T. M. Magin, R. E. Leube, R. Merkel, B. Hoffmann, *Proc. Natl. Acad. Sci. U.S.A.* **2013**, *110*, 18513.
- [15] S. Kasas, G. Longo, G. Dietler, *J. Phys. D: Appl. Phys.* **2013**, *46*, 133001.
- [16] L. Andolfi, E. Bourkoulou, E. Migliorini, A. Palma, A. Pucer, M. Skrap, G. Scoles, A. P. Beltrami, D. Cesselli, M. Lazzarino, *PLoS One.* **2014**, *9*, 112582.
- [17] Y. Qi, L. Andolfi, F. Frattini, F. Mayer, M. Lazzarino, J. Hu, *Nat. Commun.* **2015**, *6*, 8512.
- [18] K. Haase, A. E. Pelling, *J. R. Soc. Interface.* **2015**, *12*, 20140970.
- [19] G. Lamour, M. Malo, R. Crépin, J. Pelta, S. Labdi, C. Campillo, *ACS Biomater. Sci. Eng.* **2024**, *10*, 1364.
- [20] E. Herardot, M. Liboz, G. Lamour, M. Malo, A. Plancheron, W. Habeler, C. Geiger, E. Frank, C. Campillo, C. Monville, K. Ben M'Barek, *Stem Cell Rev and Rep* **2024**, *20*, 1340.
- [21] F. Rico, P. Roca-Cusachs, N. Gavara, R. Farré, M. Rotger, D. Navajas, *Phys. Rev. E.* **2005**, *72*, 021914.
- [22] R. Garcia, *Chem. Soc. Rev.* **2020**, *49*, 5850.
- [23] N. Mandriota, C. Friedsam, J. A. Jones-Molina, K. V. Tatem, D. E. Ingber, O. Sahin, *Nat. Mater.* **2019**, *18*, 1071.
- [24] O. Markova, C. Clanet, J. Husson, *Biophys. J.* **2024**, *123*, 210.
- [25] A. Battistella, L. Andolfi, M. Zanetti, S. Dal Zilio, M. Stebel, G. Ricci, M. Lazzarino, *Bioengineering & Transla Med.* **2022**, *7*, 10294.
- [26] L. Andolfi, E. Masiero, E. Giolo, M. Martinelli, S. Luppi, S. dal Zilio, I. Delfino, R. Bortul, M. Zweyer, G. Ricci, M. Lazzarino, *Integrative Biology.* **2016**, *8*, 886.
- [27] J. K. Choi, T. Yue, H. Huang, G. Zhao, M. Zhang, X. He, *Cryobiology.* **2015**, *71*, 350.
- [28] E. Giolo, M. Martinelli, S. Luppi, F. Romano, G. Ricci, M. Lazzarino, L. Andolfi, *Eur. Biophys. J.* **2019**, *48*, 585.
- [29] T. Shen, E. Benet, S. L. Sridhar, J. Abadie, E. Piat, F. J. Vernerey, *Acta Biomater.* **2019**, *85*, 253.
- [30] L. Andolfi, S. L. M. Greco, D. Tierno, R. Chignola, M. Martinelli, E. Giolo, S. Luppi, I. Delfino, M. Zanetti, A. Battistella, G. Baldini, G. Ricci, M. Lazzarino, *Acta Biomater.* **2019**, *94*, 505.
- [31] A. Chaigne, C. Campillo, R. Voituriez, N. S. Gov, C. Sykes, M.-H. Verlhac, M.-E. Terret, *Nat. Commun.* **2016**, *7*, 10253.
- [32] R. Bulteau, L. Barbier, G. Lamour, T. Pilot, E. Labrune, C. Campillo, M.-E. Terret, in *Cell Cycle Control*, (Eds: A. Castro, B. Lacroix), Springer US, New York, NY **2024**.
- [33] G. G. Bilodeau, *J. Appl. Mech.* **1992**, *59*, 519.
- [34] G. Lamour, A. Allard, J. Pelta, S. Labdi, M. Lenz, C. Campillo, *Phys. Rev. X.* **2020**, *10*, 011031.
- [35] A. Cordes, H. Witt, A. Gallemí-Pérez, B. Brückner, F. Grimm, M. Vache, T. Oswald, J. Bodenschatz, D. Flormann, F. Lautenschläger, M. Tarantola, A. Janshoff, *Phys. Rev. Lett.* **2020**, *125*, 068101.
- [36] H. Wang, Y. Li, J. Yang, X. Duan, P. Kalab, S. X. Sun, R. Li, *Sci. Adv.* **2020**, *6*, aaz5004.
- [37] D. Cimdodomo, G. Fabozzi, A. Vaiarelli, N. Ubaldi, F. M. Ubaldi, L. Rienzi, *Front. Endocrinol.* **2018**, *9*, 327.

- [38] E. E. Telfer, J. Grosbois, Y. L. Odey, R. Rosario, R. A. Anderson, *Physiol. Rev.* **2023**, *103*, 2623.
- [39] C. Charalambous, A. Webster, M. Schuh, *Nat. Rev. Mol. Cell Biol.* **2023**, *24*, 27.
- [40] F. Eghiaian, A. Rigato, S. Scheuring, *Biophys. J.* **2015**, *108*, 1330.
- [41] C. G. Muresan, Z. G. Sun, V. Yadav, A. P. Tabatabai, L. Lanier, J. H. Kim, T. Kim, M. P. Murrell, *Nat. Commun.* **2022**, *13*, 7008.
- [42] E. Fischer-Friedrich, A. A. Hyman, F. Jülicher, D. J. Müller, J. Helenius, *Sci. Rep.* **2014**, *4*, 6213.
- [43] K. M. Young, C. Xu, K. Ahkee, R. Mezencev, S. P. Swingle, T. Yu, A. Paikeday, C. Kim, J. F. McDonald, P. Qiu, T. Sulchek, *iScience.* **2023**, *26*, 106393.
- [44] P. Palay, D. Fathi, R. Fathi, *Biol. Reprod.* **2023**, *108*, 393.
- [45] X. Liu, J. Shi, Z. Zong, K.-T. Wan, Y. Sun, *Ann. Biomed. Eng.* **2012**, *40*, 2122.
- [46] X. Liu, R. Fernandes, A. Jurisicova, R. F. Casper, Y. Sun, *Lab Chip.* **2010**, *10*, 2154.
- [47] I. Krause, U. Pohler, S. Grosse, O. Shebl, E. Petek, A. Chandra, T. Ebner, *Fertility and Sterility.* **2016**, *106*, 1101.
- [48] M. L. Gardel, J. H. Shin, F. C. MacKintosh, L. Mahadevan, P. Matsudaira, D. A. Weitz, *Science.* **2004**, *304*, 1301.
- [49] E. Nikalayevich, G. Letort, G. De Labbey, E. Todisco, A. Shihabi, H. Turlier, R. Voituriez, M. Yahiatene, X. Pollet-Villard, M. Innocenti, M. Schuh, M.-E. Terret, M.-H. Verlhac, *Dev. Cell.* **2024**, *59*, 841.
- [50] A.-C. Reymann, R. Boujemaa-Paterski, J.-L. Martiel, C. Guérin, W. Cao, H. F. Chin, E. M. De La Cruz, M. Théry, L. Blanchoin, *Science.* **2012**, *336*, 1310.
- [51] B. A. Truong Quang, R. Peters, D. A. D. Cassani, P. Chugh, A. G. Clark, M. Agnew, G. Charras, E. K. Paluch, *Nat. Commun.* **2021**, *12*, 6511.
- [52] A. Touhami, B. Nysten, Y. F. Dufrêne, *Langmuir.* **2003**, *19*, 4539.
- [53] J. E. Sader, I. Larson, P. Mulvaney, L. R. White, *Rev. Sci. Instrum.* **1995**, *66*, 3789.
- [54] P.-H. Wu, D. R.-B. Aroush, A. Asnacios, W.-C. Chen, M. E. Dokukin, B. L. Doss, P. Durand-Smet, A. Ekpenyong, J. Guck, N. V. Guz, P. A. Janmey, J. S. H. Lee, N. M. Moore, A. Ott, Y.-C. Poh, R. Ros, M. Sander, I. Sokolov, J. R. Staunton, N. Wang, G. Whyte, D. Wirtz, *Nat. Methods.* **2018**, *15*, 491.
- [55] M.-H. Verlhac, J. Z. Kubiak, H. J. Clarke, B. Maro, *Development.* **1994**, *120*, 1017.
- [56] A. Reis, H.-Y. Chang, M. Levasseur, K. T. Jones, *Nat. Cell Biol.* **2006**, *8*, 539.
- [57] E. Borsuk, J. Z. Kubiak, in *Mouse Oocyte Development*, (Eds: M.-H. Verlhac, M.-E. Terret), Springer, New York, NY **2018**.
- [58] M. Almonacid, in *Mouse Oocyte Development*, (Eds: M.-H. Verlhac, M.-E. Terret), Springer, New York, NY **2018**.
- [59] S. Louvet, J. Aghion, A. Santa-Maria, P. Mangeat, B. Maro, *Developmental Biology.* **1996**, *177*, 568.
- [60] M. E. Terret, C. Lefebvre, A. Djiane, P. Rassinier, J. Moreau, B. Maro, M.-H. Verlhac, *Development.* **2003**, *130*, 5169.
- [61] M.-H. Verlhac, C. Lefebvre, J. Z. Kubiak, M. Umbhauer, P. Rassinier, W. Colledge, B. Maro, *EMBO J.* **2000**, *19*, 6065.
- [62] S. Lê, J. Josse, F. Husson, *J. Stat. Soft.* **2008**, *25*, 1.
- [63] A. Kassambara, F. Mundt, Factoextra: Extract and Visualize the Results of Multivariate Data Analyses, **2020**, <https://github.com/kassambara/factoextra>.